Raman Spectroscopic Study on the Solvation of *p*-Aminobenzonitrile in Supercritical Water and Methanol

K. Osawa,[†] T. Hamamoto,[‡] T. Fujisawa,[†] M. Terazima,[†] H Sato,[§] and Y. Kimura*,[†]

Department of Chemistry, Graduate School of Science, Kyoto University, Kyoto 606-8502, Japan, Department of Chemistry, Faculty of Science, Kyoto University, Kyoto 606-8502, Japan, and Department of Molecular Engineering, Graduate School of Engineering, Kyoto University, Kyoto 615-8510, Japan

Received: December 17, 2008; Revised Manuscript Received: February 8, 2009

Raman spectra of the C≡N stretching vibration of *p*-aminobenzonitrile (ABN) have been investigated in water, methanol, and cyclohexane under sub- and supercritical conditions, and in acetonitrile under subcritical condition. In all solvent fluids covering the supercritical region, the vibrational frequency of the C≡N stretching mode decreased with increasing solvent density from the gaseous region to the medium density region $\rho_r \cong 2$, where ρ_r is the reduced density by the critical density of the solvent. However, from the medium density region to the higher density region, the vibrational frequency turned to increase with the solvent density. The temperature-induced low frequency shift of the C≡N stretching Raman band was also ascertained by the measurement of the temperature dependence of Raman spectrum of ABN vapor above 543 K. The electronic absorption spectra in the UV region of ABN were also measured under the same experimental conditions. The absorption peak energies decreased with an increase of the solvent density, except in water above $\rho_r = 2.8$. The vibrational frequency shift in cyclohexane was explained by a sum of contributions of the repulsive interaction, the mean field attractive interaction, and the pure temperature effect probably due to the hot-band contribution. The residual frequency shift after the subtraction of the repulsive and temperature effects in water and methanol showed the low frequency shift with increasing solvent density from $\rho_r \cong 0$ to 2.8. However, above $\rho_r \cong 2.8$ in water, the residual shift showed a high frequency shift with increasing solvent density. The electronic state calculations based on the PCM model using the density functional theory (DFT) indicated that the solvent polarity change caused the low frequency shift of the C≡N stretching mode, which was also correlated with the shift of the electronic absorption spectrum. The results of the DFT calculations on the cluster of ABN with water molecules and the molecular dynamics simulations indicated that the high frequency shift of the C≡N stretching mode in water above $\rho_r \cong 2.8$ could be due to the hydrogen bonding between water and ABN.

1. Introduction

Supercritical water and supercritical alcohols have been attracting much attention for their unique properties for chemical applications.[1−5] To understand chemical processes occurring in these media, knowledge of intermolecular interactions such as solute−solvent hydrogen bonding is quite important. Among various kinds of spectroscopic methods utilized to investigate the properties of these fluids,[6−18] Raman spectroscopy is a powerful tool to understand the local solvent effect on the solute molecule such as hydrogen bonding. In our previous work, we have applied resonance and nonresonance Raman spectroscopic methods to *p*-nitroaniline (PNA) in supercritical water and supercritical alcohols.[18] PNA is a typical push−pull type molecule whose solvatochromic shift has been investigated in supercritical water by Oka et al.[17] By using the Raman spectroscopic method, we investigated mainly two vibrational modes: the NO_2 stretching vibration and the NH_2 stretching vibration.[18] The Raman band assigned to the NO_2 stretching vibration was found to be strongly dependent on the solvent polarity. The changes of the molecular geometry and the electronic structure of the ground state due to the solvation were keys to understanding the observed spectral change. On the other hand, the NH_2 stretching vibration was affected by the hydrogen bonding, and it was found that the hydrogen bonding between solute and solvent exists even under the supercritical condition of alcohols, in contrast to the prediction from the β-value estimated from the solvatochromic shift.[13]

SCHEME 1: Molecular Structure of ABN

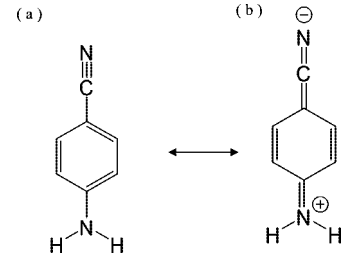

In this Article, we will present a detailed investigation of the C≡N stretching mode of *p*-aminobenzonitrile (ABN, see Scheme 1) under supercritical and subcritical conditions of water and methanol. Supercritical cyclohexane and subcritical acetonitrile were also used as nonpolar and polar aprotic references, respectively. ABN is another class of push−pull type molecules, whose spectroscopic properties have been investigated under

* Corresponding author. Phone: 075-753-4024. Fax: 075-753-4000. E-mail: ykimura@kuchem.kyoto-u.ac.jp.
[†] Department of Chemistry, Graduate School of Science.
[‡] Department of Chemistry, Faculty of Science.
[§] Department of Molecular Engineering, Graduate School of Engineering.

10.1021/jp8111606 CCC: $40.75
Published on Web 03/10/2009

various conditions such as supersonic jet clusters[19−24] or solutions.[25−29] All of these studies suggested that the hydrogen bonding between ABN and water will strongly affect the vibrational frequency of the C≡N stretching mode of ABN. For example,[27−29] several earlier studies on hydrogen-bonded clusters of ABN (or related compounds) and water molecules have indicated unique behavior of the C≡N stretching vibration and cluster configurations.[22,30] Ishikawa et al. studied the jet-cooled clusters of benzonitrile (BN) with water or methanol and found that the vibrational frequency of C≡N stretching mode is strongly dependent on the number of water molecules in the cluster.[30] The studies on the jet-cooled cluster of ABN with water or methanol also revealed that there are several stable clusters forming the hydrogen bonding between water and ABN,[22] and that the direction of the frequency shift of the NH_2 stretching mode is strongly dependent on the configuration of the cluster, although the authors did not refer to the vibrational frequency of the C≡N stretching mode.

To our best knowledge, there is no detailed report of the solvent effect on the C≡N stretching mode of ABN so far. However, the C≡N stretching mode of acetonitrile has been studied extensively under various conditions.[31−34] Ben-Amotz et al. discussed the pressure effect on the vibrational frequency of the C≡N stretching mode in various solvents in terms of the repulsive interaction and the attractive interaction between solvent and solute molecules.[32] They used a hard diatomic model in a hard-sphere solvent to estimate the repulsive solvent effect on the frequency shift, which increases the vibrational frequency. The attractive interaction was approximated by the mean field, and it was found that this interaction caused the low frequency shift. The observed frequency shift was well explained by the competition of these two effects. Later, Reimers and Hall discussed the solvent effect on the C≡N stretching mode of acetonitrile in various solvents in more detail.[33] They used a model similar to that proposed by Ben-Amotz, but they divided the attractive solvent effects into the polarity effect modeled by the reaction field of the solvent and the specific solvent effect such as hydrogen bonding. They found that the linear hydrogen bonding of water to the C≡N site contributed to the high frequency shift, which was supported by DFT or MP2 calculations on a model cluster between acetonitrile and water. Although little is known about solvent effect on the C≡N stretching mode of ABN, these findings of acetonitrile are quite helpful. Because ABN has more hydrogen-bonding sites than does acetonitrile, the appearance of the hydrogen-bonding effect will be much more complicated as is demonstrated by the cluster experiments.[30] The study on ABN will reveal another feature of the solute−solvent hydrogen bonding, which was not seen in the case of PNA.

This Article is organized as follows. In section 2, we will describe the details of experimental methods and computational methods used here. In section 3, the Raman spectra of the C≡N stretching mode of ABN will be presented, which is measured in water, methanol, and reference solvents under the supercritical and subcritical conditions. The UV absorption spectra will also be presented under the same experimental conditions. In section 4, the experimentally observed Raman shift will be discussed in a way similar to that presented for acetonitrile. We have found the hydrogen bonding in water brings a quite unique solvent effect to the frequency shift of the C≡N stretching mode.

2. Experimental Section

2.1. Materials. *p*-Aminobenzonitrile (ABN) was purchased from Tokyo Chemical Ind. Co., Ltd. and Sigma Aldrich Inc., and recrystallized from ethanol before use. Methanol, cyclohexane, benzene, tetrahydrofuran, and acetonitrile (all solvents are of spectra grade) were purchased from Nacalai Tesque and Wako Chemicals and used without further purification. Ion-exchanged water produced by a Milli-Q system (>18 Ω cm^{-1}) was used.

2.2. Apparatus. The experimental setup for the Raman spectral measurements under the nonresonant condition in supercritical fluids has been described elsewhere.[18] Briefly, a 514.5 nm line of an Ar ion laser (Coherent: Enterprise or Coherent: Innova) was used for the Raman probe, and the Raman signal was detected in a back scattering geometry by using a high-temperature and high-pressure optical cell specially designed for the Raman measurement.[35] The sample solution continuously bubbled by argon gas was flowed into the high-pressure cell at a rate of 1.0−1.5 mL min^{-1} using an HPLC pump (JASCO: PU-2080plus) in a single-pass configuration. The pressure of the fluid was controlled by a back pressure regulator (JASCO: 880-81) with an accuracy of about ±0.3 MPa. The temperature of the cell was regulated within the accuracy of about ±1 K by a sheathed heater wounded around the cell and a thermocouple directly inserted into the sample chamber. We confirmed that ABN was stable under the supercritical condition by measuring the absorption spectrum of the sample solution before and after the flow through the high-temperature and high-pressure optical cell. To evaluate the Raman spectra of the solute molecule, we measured the spectra with and without the solute molecule successively under the same experimental condition and evaluated the difference between them. The concentration of the sample solution was prepared to be about 10 mM for water and cyclohexane, and 100 mM for methanol and acetonitrile, respectively. Raman spectra were recorded under the following conditions; in water (T_c (critical temperature) = 647 K, P_c (critical pressure) = 22.1 MPa) along the 40.0 MPa isobar (between 297 and 664 K) and the 664 K isotherm (between 40.0 and 18.9 MPa); in methanol (T_c = 513 K, P_c = 8.10 MPa) along the 40.0 MPa isobar (between 297 and 538 K) and the 538 K isotherm (between 40.0 and 7.6 MPa); in cyclohexane (T_c = 553 K, P_c = 4.07 MPa) along the 30.0 MPa isobar (between 297 and 593 K) and the 593 K isotherm (between 30.0 and 6.1 MPa); in acetonitrile (T_c = 545 K, P_c = 4.83 MPa) along the 40.0 MPa isobar (between 297 and 423 K). The densities at different temperatures and pressures were calculated by empirical equations of state.[36]

The absorption spectra under the high-pressure and high-temperature conditions were measured using a D2 lamp (Otsuka electronics, Model MC-964) as a light source, and the transmission intensities of the light with and without the solute were successively measured by an electronically cooled CCD camera (Princeton: Insight 256E).

For the measurement of Raman and absorption spectra of ABN at vapor, ABN was enclosed in a quartz cell, which was sealed after the evacuation to 2×10^{-4} torr. The cell was placed in an air bath equipped with quartz optical windows. The air bath was a rectangular parallelepiped made of brass plates with 12 mm thickness, and there was a space inside the bath to place a 1 cm quartz cell. The bath was covered by plates of insulator, and the temperature was monitored by a thermocouple and controlled by two cartridge heaters immersed into brass plates. The Raman and absorption spectra of ABN vapor were measured by the same systems used for the high-temperature and high-pressure measurements. For these measurements, the signals at room temperature were used as background signals.

2.3. Computational Method. The ground-state geometrical optimization and normal-mode analysis of ABN were performed by the density functional theory (DFT) at the level B3LYP using the basis set 6-31+G(d,p) as implemented in Gaussian 03.[37] The polarizable continuum model (PCM)[38,39] and cluster model were used to include the solvent effects. To estimate the anharmonic coefficients of the C≡N vibrational mode of acetonitrile and ABN, we performed the vibrational SCF (VSCF) calculations implemented in GAMESS.[40] We used the DFT theory at the level of B3LYP and used the smaller basis set function midi! to save computational time. The anharmonic potential was calculated by the quartic force field (QFF) method.

Molecular dynamics simulations of ABN in water have been performed using LAMMPS.[41] We employed the SPC/E model of water[42] and the SHAKE algorithm to fix the water structure. OPLS/AA potential parameters were employed for the intermolecular potential parameters between water and ABN,[43] and intramolecular geometry of ABN was fixed during the simulations. Simulations were performed using one ABN molecule and 512 water molecules by the NVT ensemble with the periodic boundary condition. The equations of motion were integrated by the velocity Verlet method, and the Nose thermostat was applied with the time constant of 0.1 ps. The Coulomb interaction was treated by the Ewald method, and the short-ranged interaction was cut off at 9.0 Å. The time step was 1 fs, and after the initial 50 ps for the equilibration the solvation structure of water around ABN was analyzed by the data of the following 4 ns, and the trajectory data were collected every 1 ps. Sets of number density and temperature are listed in Table 5.

3. Results

3.1. Raman Spectra of ABN for the C≡N Stretching Mode. Figure 1a−d shows Raman spectra of the C≡N stretching mode of ABN (ν_{CN}) at various pressures and temperatures in (a) water, (b) methanol, (c) cyclohexane, and (d) acetonitrile, respectively. The band shape is asymmetrical near room temperature in water and methanol, and it becomes symmetrical at elevated temperatures. The behavior is quite similar to those observed for the C≡N stretching mode of acetonitrile in water and methanol.[31] Eaton et al. measured the IR spectrum of acetonitrile in methanol and found that the band is double peaked and that the relative intensity is strongly dependent on the temperature; that is, the double peaks are merged into a single band with increasing temperature from 233 to 323 K.[31] They considered that the higher frequency band is due to the hydrogen-bonded one and the lower one to the not-strongly interacting one. In the present case, the asymmetrical feature is weakened with increasing temperature as was observed for the case of acetonitrile. Therefore, we also consider that the asymmetry is due to the hydrogen-bonding effect. The band shape is almost symmetrical along the isobar in all solvents.

In water, from 301 to 664 K along the 40.0 MPa isobar (Figure 1a), the band shows the low frequency shift as was observed previously for the C≡N stretching mode of acetonitrile.[31] On the other hand, from 40.0 to 18.9 MPa along the isotherm, the band shows the high frequency shift. In methanol (Figure 1b), the low frequency shift along the isobar is not clearly observed due to its complex band shape, although a high frequency shift similar to that in water is observed along the isotherm. In cyclohexane (Figure 1c), the profile of the spectral shift is similar to that in water, although the variation is not so large. In acetonitrile (Figure 1d), the shift of the spectra is small within the temperature range studied here. Because of the instability of acetonitrile at high temperatures, the experiment in acetonitrile was limited below 423 K.

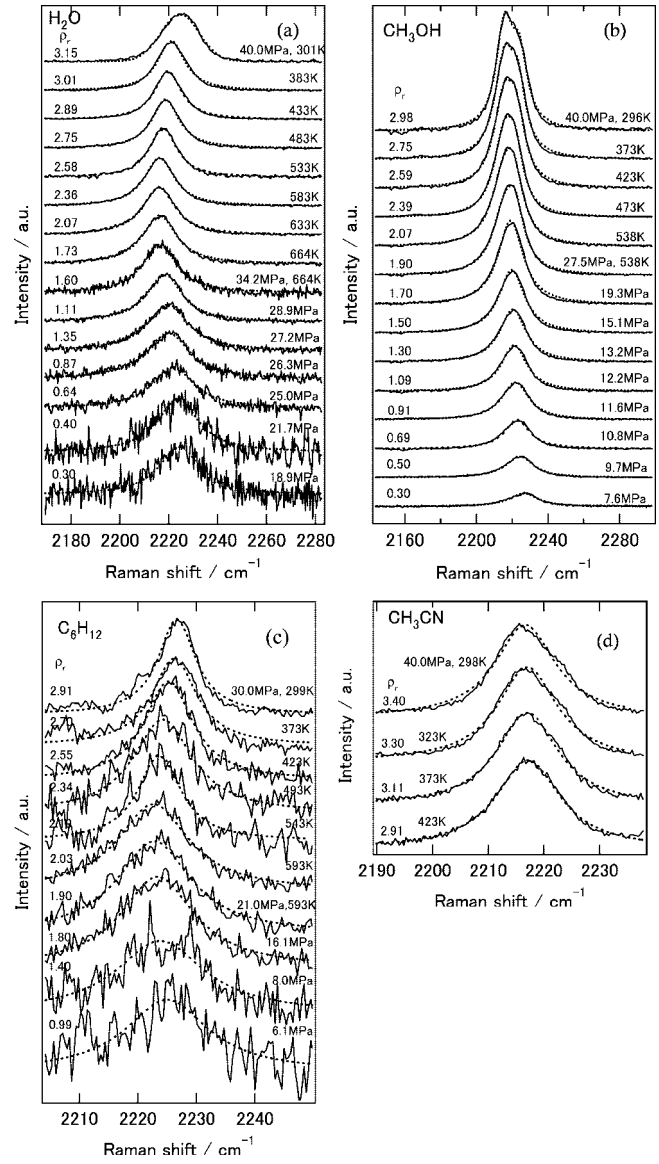

Figure 1. Raman spectra of C≡N stretching mode of ABN at different temperatures and pressures in (a) water, (b) methanol, (c) cyclohexane, and (d) acetonitrile, respectively. Solid lines are observed spectra, and dashed lines are the fits to the spectra.

It has been suggested that there is a hot-band contribution to the band assigned to the C≡N stretching mode of acetonitrile.[33,44−46] According to Fini and Mirone, the frequency of the C≡N stretching mode may be 5 cm^{-1} lower in frequency if the lower frequency band (369 cm^{-1}) is populated.[44] If a similar effect is present for ABN, the variation of ν_{CN} along the isobar may contain the effect of the hot-band, which is independent of the solvent. To test this possibility, we measured the temperature effect on the Raman band of ABN without solvent. Figure 2 shows the Raman spectra of ABN in the vapor phase around the C≡N stretching region at different temperatures. Below 543 K, we could not obtain the signal due to the low vapor pressure of ABN. The peak position shifts to the low frequency with increasing temperature. Therefore, we considered that a hot-band contribution affects the band shape and the apparent peak position of ABN.

Figure 3 shows the plot of the band peaks of C≡N stretching mode (ν_{CN}) against the reduced density of the solvent (ρ_r =

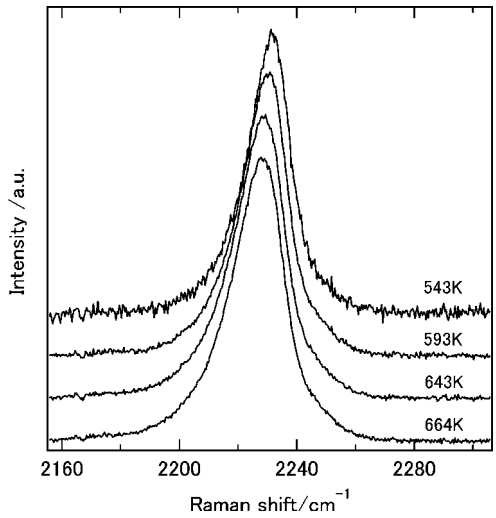

Figure 2. Raman spectra of C≡N stretching mode of ABN in vapor at different temperatures from 543 to 693 K.

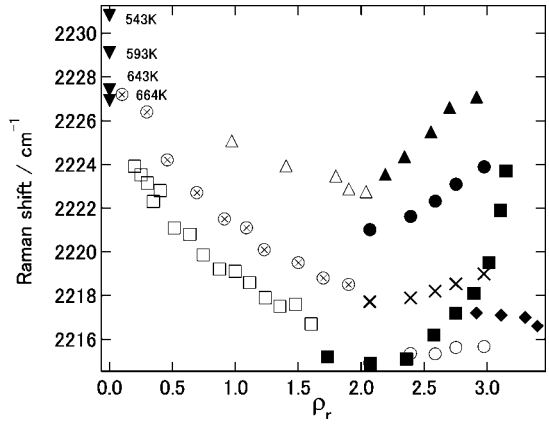

Figure 3. The plot of the peak frequency of the C≡N stretching mode (ν_{CN}) against the reduced density of the solvent; ■, in water from ambient to 664 K at 40.0 MPa (corresponding temperatures and reduced densities are shown in Figure 1a); □, in water at 664 K; ●, in methanol from ambient to 538 K at 40.0 MPa (higher peak) (corresponding temperatures and reduced densities are shown in Figure 1b); ○, in methanol from ambient to 538 K at 40.0 MPa (lower peak); ×, the averaged values of the higher peak and the lower peak in methanol; ⊗, in methanol at 538 K;▲, in cyclohexane from ambient to 593 K at 30.0 MPa (corresponding temperatures and reduced densities are shown in Figure 1c); Δ, in cyclohexane at 593 K; ◆, in acetonitrile from ambient to 323 K at 40.0 MPa (corresponding temperatures and reduced densities are shown in Figure 1d);▼ (at $\rho_r = 0$), in vapor.

ρ/ρ_c, where ρ_c denotes the critical density). To determine ν_{CN}, we fit the Raman band to a Lorentzian function. In water at 301 K, the band shape could not be simulated by a Lorentzian function. However, because a Gaussian function reproduced the spectrum well, we used this function for the peak position estimation. In methanol, two Lorentzian functions were employed to fit the spectra obtained along the isobar (temperature change). The fitting was performed from the low temperature to the high temperature by using the parameters obtained at the lower temperature as initial guesses. Along the isotherm at the supercritical temperature, the band became almost symmetrical, and it was impossible to simulate the band with two Lorentzian functions. In this case, a single function was employed. The fitted curves are shown by the broken lines in Figure 1a−d, which simulate the observed spectrum quite well. In all solvents covering the supercritical region, ν_{CN} shows a V-shape dependence on the density (Figure 3); that is, from the gaseous phase to the medium density region around $\rho_r = 2.0$, ν_{CN} decreases with increasing solvent density at the constant temperature. On the other hand, from the medium density to the higher density region ($\rho_r = 3.0$) mostly along the isobar, ν_{CN} increases with increasing solvent density by decreasing the temperature. The density dependence in the lower density region below $\rho_r \cong 0.5$ becomes larger in the order of cyclohexane, methanol, and water. The density dependence on the higher density region along the isobar also follows the same order. In methanol, there is an apparent discontinuity of the peak position around $\rho_r = 2.0$. It is to be noted that in the region of isobar only the higher frequency peak shows a shift and that the lower frequency peak is almost constant. The discontinuity is artificial because the band decomposition may not be unique at the elevated temperature. In the figure, we also plotted the weighted average of two peak positions (×) by their areas. As is shown in the figure, averaged peak position is smoothly connected to the results in supercritical methanol. In acetonitrile, from 298 to 423 K along the 40.0 MPa isobar, ν_{CN} shows little lower-frequency shift, which makes a good contrast to the cases to other solvents. We have also plotted the density dependence of the vibrational bandwidth of ν_{CN} estimated by the fitting in the Supporting Information (Figure S1). In all solvents, the bandwidths increase with decreasing density. The bandwidth in cyclohexane is the narrowest in all solvents, and those of the other three solvents are similar to one another at the same reduced density.

The density dependences of the Raman spectra of other vibrational modes in methanol and water in the fingerprint region are given in the Supporting Information (Figures S2 and S3). The CH bending vibration, phenyl−CH stretching vibration, and ring C=C stretching vibration have been detected, and their density dependences of the peak positions were analyzed. The density dependence in the isothermal region is different from that in the isobar region as is observed for the C≡N stretching mode. However, the magnitude of the shift is rather smaller than the C≡N stretching mode, and the detailed analysis is difficult.

3.2. UV Absorption Spectra of ABN. The solvatochromic shift of the UV absorption of ABN is informative to clarify the solvent polarity around an ABN molecule. In the UV region, ABN shows a strong absorption band around 270 nm with a shoulder band extended to the longer wavelength region. The main band was assigned to the benzene ^1L_a absorption band, with a large amount of charge transfer (CT) character due to the existence of the donor and acceptor substituents.[25,26] The shoulder band was assigned to the ^1L_b absorption band, which has less CT character. Therefore, the transition energy to the S_2 state (^1L_a band) is strongly influenced by the solvent polarity. Figure 4a−d shows the absorption spectra of ABN in (a) water, (b) methanol, (c) cyclohexane, and (d) acetonitrile, respectively. As is shown in Figure 4a, the absorption spectrum in water once shows a red shift with increasing temperature from the ambient condition (or decreasing the density) and then shows a blue shift with decreasing density at constant temperature. On the contrary to this, the spectra in methanol, cyclohexane, and acetonitrile show a continuous blue shift with decreasing density from the ambient condition.

Figure 5 shows the density dependence of the peak position in water, methanol, acetonitrile, and cyclohexane. The absorption band peak (ω_{abs}) was determined by fitting the top of the spectrum to a Gaussian function. As is shown in Figure 5, the density dependences of the absorption peak positions in water and methanol from the gaseous region to $\rho_r = 1.5$ are quite similar to each other. The density dependence below $\rho_r \cong 0.5$

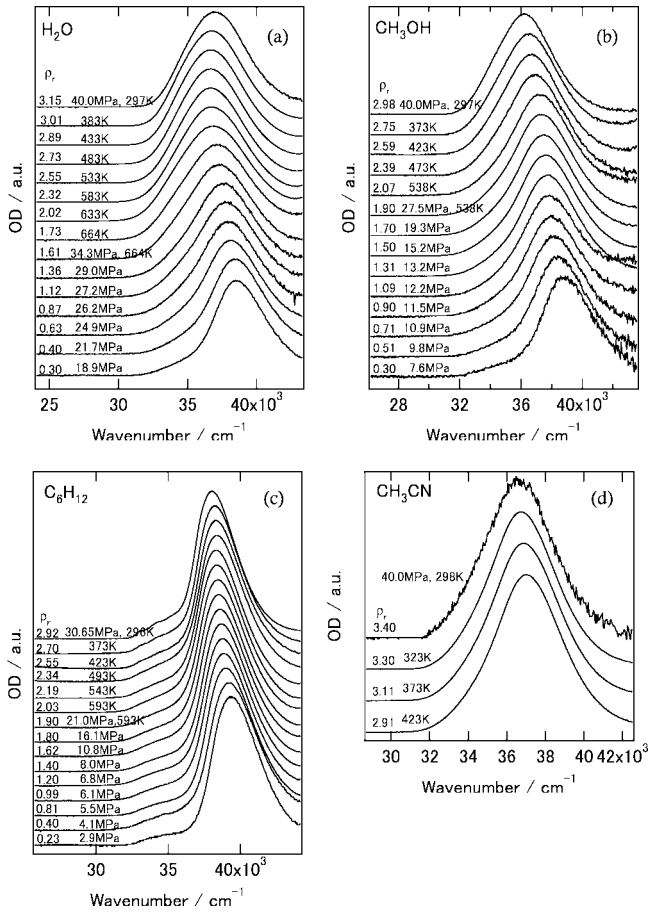

Figure 4. UV absorption spectra of ABN at different temperatures and pressures in (a) water, (b) methanol, (c) cyclohexane, and (d) acetonitrile, respectively.

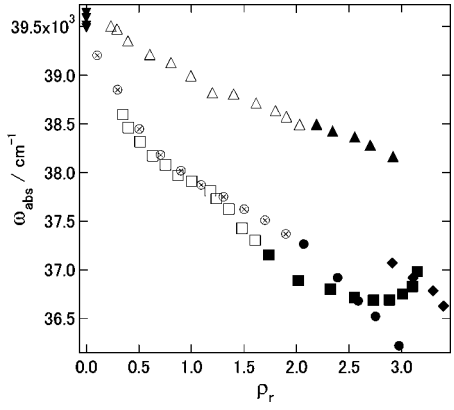

Figure 5. The plot of the absorption peak (ω_{abs}) of ABN against the reduced density of the solvent. The notations of the symbols are the same as in Figure 3, except for ●, which represents peak value in methanol under isobaric condition.

is much larger than that in the higher density region, which is the characteristic behavior of the local density enhancement of supercritical fluids.[47] On the other hand, the solvatochromic shift in cyclohexane is much smaller than those in water and methanol, and the effect of the local density enhancement is hardly detected. At the higher density region above $\rho_r = 2.7$, the absorption peak in water increases with increasing solvent density.

In the Supporting Information (Figure S4), we have presented the density dependence of the bandwidths of the absorption spectra. The bandwidths were very broad in hydrogen-bonding solvents (water and methanol), even in the low density region of $\rho_r = 0.3$. The large dependence of the absorption bandwidth on the solvent species even in the low density region was also reported for the case of comarine 153,[48] although the difference is more significant in the present case.

4. Discussion

4.1. Solvent Effects on ν_{CN}. The vibrational frequency shift of the C≡N stretching mode of acetonitrile has been discussed by several authors as was mentioned in the Introduction, and the vibrational frequency shift relative to the gaseous phase ($\Delta\nu$) is generally divided into four factors as follows:[33] the frequency shift brought by the temperature effect ($\Delta\nu_T$), the short-range repulsive interaction ($\Delta\nu_R$), the long-range attractive interaction

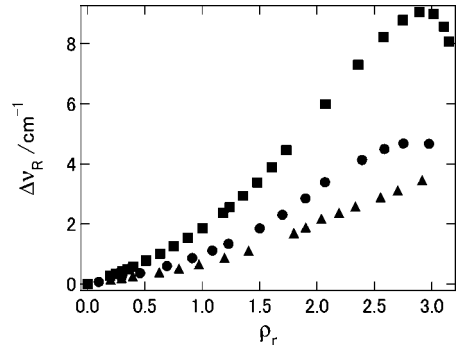

Figure 6. The density dependence of $\Delta\nu_R$ calculated by the hard-sphere diatomic model for the corresponding thermodynamic states measured experimentally: ■, in water; ●, in methanol; ▲, in cyclohexane.

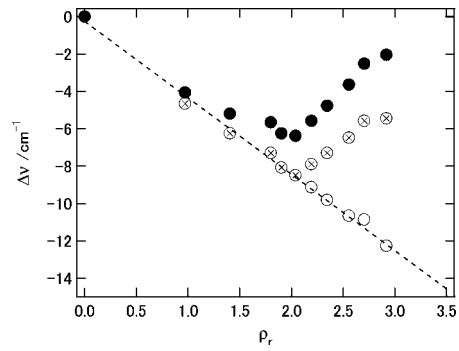

Figure 7. Solvent density dependence of $\Delta\nu$ (●), $\Delta\nu - \Delta\nu_R$ (⊗), and $\Delta\nu_A + \Delta\nu_{HB}$ (○) ($=\Delta\nu - \Delta\nu_R - \Delta\nu_T$) in cyclohexane. The standard frequency in vapor used to estimate the relative shift is the value at 593 K.

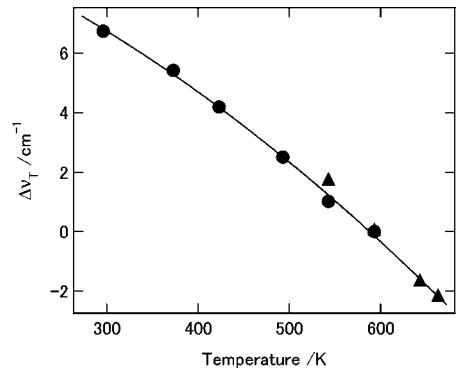

Figure 8. The relative shift of the C≡N stretching peak frequency at different temperature to the value at 593 K in vapor: ●, estimated shift from the analysis of the peak shift in cyclohexane; ▲, observed shift in vapor.

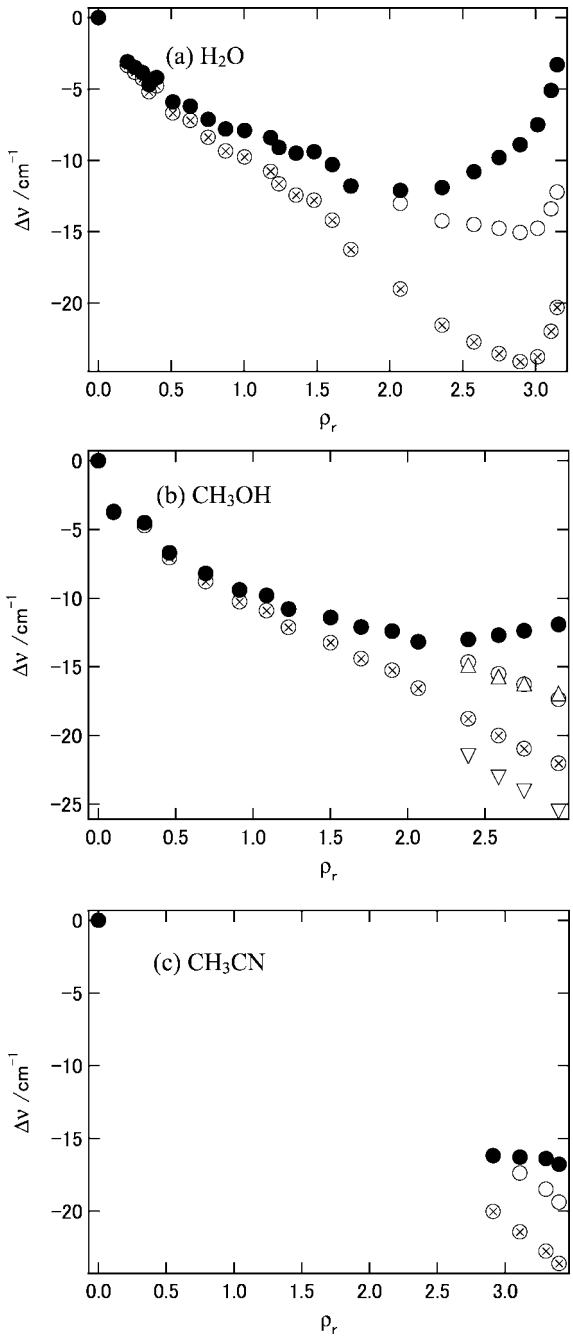

Figure 9. Solvent density dependence of $\Delta\nu$ (●), $\Delta\nu - \Delta\nu_T$ (○), and $\Delta\nu_A + \Delta\nu_{HB}$ (⊗) (=$\Delta\nu - \Delta\nu_R - \Delta\nu_T$) in (a) water, (b) methanol, and (c) acetonitrile, respectively. In methanol under isobar condition, the values of $\Delta\nu_A + \Delta\nu_{HB}$ for the higher (△) and lower (▽) frequency modes are also plotted beside the average value (⊗). The standard frequencies in vapor used to estimate the relative shift are the values at (a) 664 K, (b) 538 K, and (c) 323 K, respectively.

($\Delta\nu_A$), and the specific solute−solvent interaction such as the hydrogen bonding ($\Delta\nu_{HB}$):[49]

$$\Delta\nu = \Delta\nu_T + \Delta\nu_R + \Delta\nu_A + \Delta\nu_{HB} \quad (1)$$

The temperature effect is the apparent shift of the peak position due to the hot-band contribution, which is independent of the solvent. In the case of the previous studies on acetonitrile,[33] most studies on the solvent effects were done at constant temperature, and the temperature effect was not included explicitly. However, in the present case, we had to include the effect explicitly due to the wide temperature range under study (see Figure 2). The repulsive effect comes from changes in the vibrational potential curvature by the short-ranged repulsive interaction. This effect generally increases the vibrational frequency. The long-ranged attractive interaction is often treated by the dielectric continuum model and is expressed in the most simple case by using the Onsager reaction field such as:[50]

$$\Delta\nu_A \propto \frac{\varepsilon - 1}{2\varepsilon + 1} \quad (2)$$

where ε is the dielectric constant of the solvent. Generally, the vibrational frequency decreases with increasing solvent polarity. Finally, there should exist the hydrogen-bonding effect in water and methanol, and we want to extract this contribution from the observed spectrum shift in supercritical water and methanol.

For this end, at first, we tried to subtract the effect of the temperature ($\Delta\nu_T$). Unfortunately, Raman spectra below 543 K for ABN vapor could not be measured. Therefore, we used the following way to evaluate $\Delta\nu_T$. First, the effect of the repulsive interaction on $\Delta\nu_{CN}$ was determined in cyclohexane solution using the hard-sphere diatomic model employed by Ben-Amotz et al.[32] Next, the effect of the attractive interaction $\Delta\nu_A$ for cyclohexane was determined by the mean field approximation using the data obtained under the isothermal condition. Because cyclohexane does not have any hydrogen-bonding effect, the residual shift estimated for the isobaric condition (temperature change), that is, $\Delta\nu - (\Delta\nu_R + \Delta\nu_A)$, is expected to represent the pure temperature effect on the shift ($\Delta\nu_T$). Using this $\Delta\nu_T$ and $\Delta\nu_R$ estimated for each solvent, we will discuss the effects of the attractive interaction and the hydrogen bonding on $\Delta\nu$ for other hydrogen-bonding solvents such as water and methanol.

For the estimation of the repulsive interaction, we have followed the way proposed by Ben-Amotz et al.[32] They used the hard-sphere diatomic model to estimate the repulsive effect on the vibrational frequency of CH, CC, and CN stretching modes of acetonitrile. Formally, the repulsive effect is written as

$$\Delta\nu_R = \nu_0 \frac{F_R}{f}\left[-\left(\frac{3g}{2f}\right)f_1(\kappa) + \left(\frac{G_R}{F_R}\right)f_2(\kappa)\right] \quad (3)$$

where F_R and G_R are the first and second derivatives of the chemical potential of the hard diatomic molecules with respect to the bond distance, respectively. These values are calculated

TABLE 1: Parameters Used for the Estimation of the Repulsive Effect Based on the Hard-Sphere Theory[a]

	Solute Parameters[b]					
	r_0/Å	r_{eff}/Å	σ_1/Å	σ_2/Å	f/dyn cm^{-1}	r_0 (g/f)
	1.16	1.89	4.00	3.10	1 773 000	−2.77
	Solvent Parameters[c]					
	σ_s/Å	ε_{LJ}/k_B/K				
water	2.922	371				
methanol	3.835	376				
cyclohexane	5.645	554				
acetonitrile	4.244	405				

[a] r_0, bond length; r_{eff}, effective diatomic separation; σ_1, σ_2, effective diatomic diameters; f, harmonic force constant; g, anharmonic force constant; σ_s, solvent diameters; ε_{LJ}/k_B, reduced constant of attractive parameter. [b] Reference 32. [c] Reference 51.

TABLE 2: Harmonic and Anharmonic Vibrational Frequencies for Acetonitrile and ABN Calculated by VSCF[a]

	basis set	*E*/hartree	μ/D	*L*(C≡N)/Å	ν_{CN}/cm^{-1} (harmonic)	ν_{CN}/cm^{-1} (PT2-VSCF)	x_e	f/g/s^{-2}	g/f/cm^{-1}
acetonitrile	midi!	−131.930	3.53	1.1575	2375.33	2336.86	0.00810	2.15×10^6	-2.72×10^8
	6-31+G(d,p)	−132.681	4.07	1.1612	2361.99				
ABN	midi!	−377.450	6.12	1.1614	2346.18	2303.79	0.00965	2.02×10^6	-2.92×10^8
	6-31+G(d,p)	−379.650	6.96	1.1654	2324.32				

[a] *E*, calculated zero-point energy; μ, dipole moment; *L*(C≡N), C≡N bond length; x_e, anharmonic coefficient; *f*, harmonic force constant; *g*/*f*, anharmonicity ratio.

by the cavity distribution function of the model hard-sphere solution. *f* and *g* are the harmonic and the anharmonic force constants of a diatomic solute's vibrational potential in the gas phase. $f_1(\kappa)$ and $f_2(\kappa)$ are the Morse correction coefficients. For the hard-sphere parameters of the solvent, we used the values given by Ben-Amotz et al.,[51] and the calculation was performed without Morse correction coefficients ($f_1(\kappa) = f_2(\kappa) = 1$) (see Table 1). As for the parameters for the C≡N stretching mode, we used the same parameters used for acetonitrile, because the vibrational energy is localized on the C≡N part of ABN and the effect of the repulsive force on this mode is expected to be similar to that of acetonitrile. We have estimated the parameters of *f* and *g* by the DFT calculations using VSCF with a simple basis set (midi!) for acetonitrile and ABN (see section 2.3). The optimized molecular structure and the vibrational frequency are compared to those obtained by using the larger basis set (6-31+G(d,p)) in Table 2. It shows that the optimized structure by the smaller basis set is not so different from that by the larger one. The values of *f* and *g* were determined by comparing the harmonic vibrational frequency and the anharmonic frequency obtained by VSCF with the Morse potential parameters (the detail is described in the Supporting Information). The results are shown in Table 2, and the parameters are similar to each other. Therefore, employing the parameters for acetonitrile is considered to be a reasonable approximation for the estimation of the repulsive force. Figure 6 shows the estimated shift due to the repulsive interaction in each solvent. The shift monotonically increases the vibrational frequency in all solvents except for the case of water above $\rho_r = 3$. The larger effect of the water than the other two solvents is due to the large number density of the water molecule. The decrease of $\Delta\nu_R$ in water above $\rho_r = 3$ is originated from the decrease of the packing effect with decreasing temperature, because we employed a model such that the hard-sphere diameter of the solvent is dependent on the temperature.

According to the mean field approximation, the effect of the attractive interaction is expected to be linearly dependent on the solvent density.[32] For the case of supercritical fluids, this approximation is often invalid due to the local density enhancement.[47] In cyclohexane, however, the effect of the solute−solvent interaction is not strong, and the local density enhancement, which may bring the nonlinear density dependence of the spectral shift, is expected to be quite small. In fact, the frequency shift in cyclohexane after the subtraction of the effect of the repulsive interaction (in Figure 7) is almost linearly dependent on the solvent density along the isothermal condition. Therefore, we assumed that the effect of the attractive interaction in cyclohexane is estimated from the relation that

$$\Delta\nu_A = C_A\rho_r \tag{4}$$

where C_A is a proportional constant. The dashed line in Figure 7 shows the relation estimated from the results under the isothermal condition.

Finally, $\Delta\nu_T$ was determined by subtracting ($\Delta\nu_R + \Delta\nu_A$) from $\Delta\nu$ in cyclohexane. Figure 8 shows the effect of the temperature thus estimated together with the experimental data obtained in the gaseous phase. The estimated temperature effect is smoothly connected to the experimental one. Therefore, we determined the pure temperature effect on the frequency ($\Delta\nu_T$) by fitting the result in Figure 8 with a quadratic function of the temperature, which simulated the experimental results reasonably (solid line).

Now the attractive and the hydrogen-bonding effects on the vibrational frequency of the C≡N stretching mode in other solvents are estimated by subtracting the factors of $\Delta\nu_R$ and $\Delta\nu_T$ from the observed $\Delta\nu$. The results are shown in Figure 9a−c. In all solvents, the residual shift shows a negative shift from $\rho_r = 0$, except for the water above $\rho_r \cong 2.8$. From $\rho_r = 0$ to $\rho_r = 0.5$ in water and methanol, the density dependence is somewhat larger than above $\rho_r = 0.5$. At the higher density region of $\rho_r \cong 2.8$, in water, there appears an evident increase of the vibrational frequency with increasing solvent density. For the averaged value of ν_{CN} of methanol, the value simply decreases with increasing the solvent density, and no inversion of the density dependence is observed. However, the asymmetrical band shape in methanol near the room temperature suggests specific solute−solvent interaction. In fact, for the value of the higher frequency mode, the positive shift is apparent relative to the prediction from the extrapolation of the values in the medium density region. Therefore, the solvent effect, which was not included in the repulsive and mean field attractive interactions, say, the hydrogen-bonding effect, may also exist in methanol at the higher density region above $\rho_r \cong 2.5$.

4.2. Effects of the Mean Field Attractive Interaction. In all solvents covering the supercritical region, ν_{CN} decreases with increasing solvent density from the gaseous phase at the constant temperature. We consider that the shift from the low to the

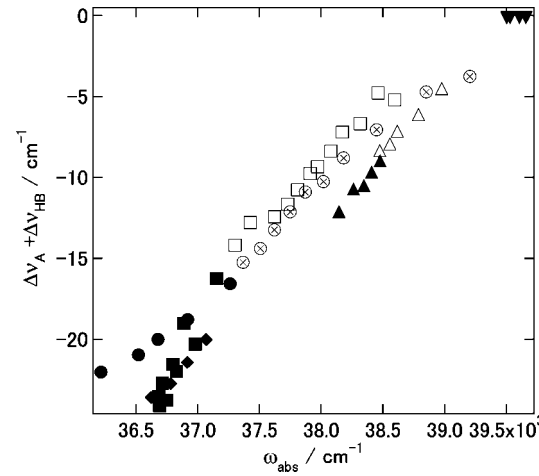

Figure 10. The correlation between the peak frequencies of the C≡N stretching mode (ν_{CN}) and the absorption spectrum (ω_{abs}). The notations of the symbols are the same as in Figure 5.

TABLE 3: Structural Information of ABN Obtained by the Geometry Optimization Using SCRF/PCM Model at the B3LYP/6-31+G(d,p) Level Calculated by DFT Theory Using Gaussian 03[a]

solvent	ε^b	$(\varepsilon - 1)/(2\varepsilon + 1)$	ΔE/kJ mol^{-1}	μ/D	θ	L(C≡N)/Å	ν_{CN}/cm^{-1} (calculated)	ν_{CN}/cm^{-1} (experimental)
vacuum	1.00	0	0.0	6.96	20.35	1.1626	2323.37	2230.9(543K)
cyclohexane	2.02	0.202	–23.1257	8.15	19.25	1.1662	2313.20	2228.6
benzene	2.25	0.227	–26.1713	8.27	19.05	1.1664	2311.35	2221.1
tetrahydrofuran	7.58	0.407	–50.5862	9.53	17.70	1.1675	2298.52	2216.6
methanol	32.6	0.477	–61.5110	10.08	16.92	1.1681	2292.06	2217.5
acetonitrile	36.6	0.480	–61.8234	10.10	16.85	1.1681	2291.78	2217.2
water	78.4	0.490	–63.7558	10.16	16.82	1.1683	2290.65	2223.5

[a] ε, dielectric constant of solvent; ΔE, stabilization energy by solvent; μ, dipole moment; θ, out-of-plane angle of the NH_2 group in deg; L(C≡N), C≡N bond length. [b] Reference 50.

medium density region ($\rho_r \cong 2$) is mainly due to the polarity effect of the solvent. This is demonstrated by the correlation between $\Delta\nu_A + \Delta\nu_{HB}$ and ω_{abs} as is shown in Figure 10. These two values are in a good linear correlation especially for the supercritical region (open symbols). As is mentioned previously, the ^1L_a absorption band has the CT character, and the spectral shift may be modeled by a similar equation such as eq 2. The linear correlation between $\Delta\nu_A + \Delta\nu_{HB}$ and ω_{abs} suggests that the solvent polarity effect will decrease the vibrational frequency of ν_{CN}. This may be understandable if we consider the resonance structures for the ground state of ABN as is shown in Scheme 1. With increasing solvent polarity, a charge-separated state of ABN (b) will be stabilized, and the bond order of C≡N may decrease.

To confirm the above idea, we performed the normal-mode analysis of ABN in a dielectric continuum solvent using the PCM model calculations implemented in the Gaussian 03 program. Typical intramolecular parameters obtained by the calculations in various solvents with different polarities are listed in Table 3. The dipole moment of ABN increases with increasing solvent polarity, which means that the contribution of the charge-separated form increases with increasing solvent polarity. The calculated normal-mode frequency shift of ν_{CN} against the one in the gaseous phase is almost linear to the solvent Onsager reaction field as shown in Table 3. The experimental results in aprotic solvents almost follow the theoretical calculations, suggesting that the effect of the polarity monotonically decreases the vibrational frequency.

To compare the polarity effect of the solvent molecule more directly, we estimated the effect of the attractive interaction by the initial slope against the solvent density (at $\rho_r = 0$) in Figure 9a–c. The slope was estimated by fitting the results to the third-order polynomial of the solvent number density in water and methanol for the isothermal data, and the linear function of the solvent density in cyclohexane and acetonitrile. Because the data in the lower-density region were not available for acetonitrile, the estimation is quite rough. The density dependences are estimated as −1.6, −3.2, −1.8, and −2.1 cm^{-1} molecule^{-1} nm^3 for water, methanol, cyclohexane, and acetonitrile, respectively. If we simply divide the relative shifts of ν_{CN} estimated by the PCM calculations to ν_{CN} in the gaseous phase by the number density of the solvent, the spectral shifts per solvent molecules are given as −1.0, −2.1, −1.8, and −2.8 cm^{-1} molecule^{-1} nm^3 for water, methanol, cyclohexane, and acetonitrile, respectively. We consider that they are in reasonable agreement despite the very rough estimation.

4.3. Effect of the Hydrogen Bonding. The high frequency shift of the C≡N stretching mode above $\rho_r \cong 2.8$ in water cannot be explained from the dielectric continuum model. Therefore, the localized effect such as the hydrogen bonding is expected to play an important role in changing the vibrational frequency. It is also to be noted here similar behavior is detected for the UV absorption peak, and both behaviors seem to be correlated with each other according to Figure 10. However, the electronic transition involves the problems in both the ground and the excited states, and the situation may be more complicated. In the present work, we do not mention the problem of the absorption behavior further.

To understand the effect of the local solvent configuration on the vibrational mode, at first we estimated how the hydrogen bonding between solute and solvent affects the vibrational frequency of the C≡N stretching mode by performing the ground-state geometry optimization and normal-mode analysis of the clusters of ABN with water molecules. We tested 1:1 clusters of ABN with water and 1:2 clusters with water. Supersonic jet experiments reported several stable 1:1 structures of ABN with water molecules.[22] Sakota et al. compared the measured IR-dip spectra of jet-cooled ABN(H_2O) complex with that calculated by ab initio calculations about the NH_2 symmetry stretching mode and assigned the structures. We started the geometrical optimization from the structures proposed by them, which are illustrated in Scheme 2a–d. A water molecule is bonded to the amino site in conformers (a) and (d). The amino group acts as a proton donor in (a) NH_2-donor conformer, where the amino proton is hydrogen bonded to the oxygen atom of water. On the other hand, a water molecule acts as a proton acceptor in (d) NH_2-acceptor conformer, where the water hydrogen is bonded to the amino nitrogen. In the conformers (b) and (c), a water molecule is bonded to the C≡N site. In the structure (b), a water molecule interacts with ABN from the side of the C≡N bond, whereas structure (c) involves the σ-type hydrogen bond between the water hydrogen and the cyano nitrogen (C≡N-linear conformer). For these conformers, DFT calculations at the B3LYP/6-31+G(d,p) level were performed.

The optimized structural parameters and ν_{CN} for these clusters are listed in Table 4 (the calculation results for the fingerprint region are also given in the Supporting Information, Table S1). It shows that ν_{CN} shifts to the high frequency for the clusters (c) and (d), while to the low frequency for (a) and (b) clusters. The low frequency shift in the structure (a) is due to the enhancement of the charge-separated state by the hydrogen bonding. The low frequency shift in the structure (b) is interpreted as the result of weakening of the C≡N bond by the water molecule, which seems to be a dipole–dipole interaction between the water and the C≡N group, and not directly linked to the hydrogen bonding. The high frequency shift in the structure (d) is due to the reduction of the contribution of the charge-separated state by making an ammonia-like structure between the hydrogen-bonded water molecule and amino group.

SCHEME 2: Structures of ABN(H_2O) and ABN(H_2O)$_2$ Clusters[a]

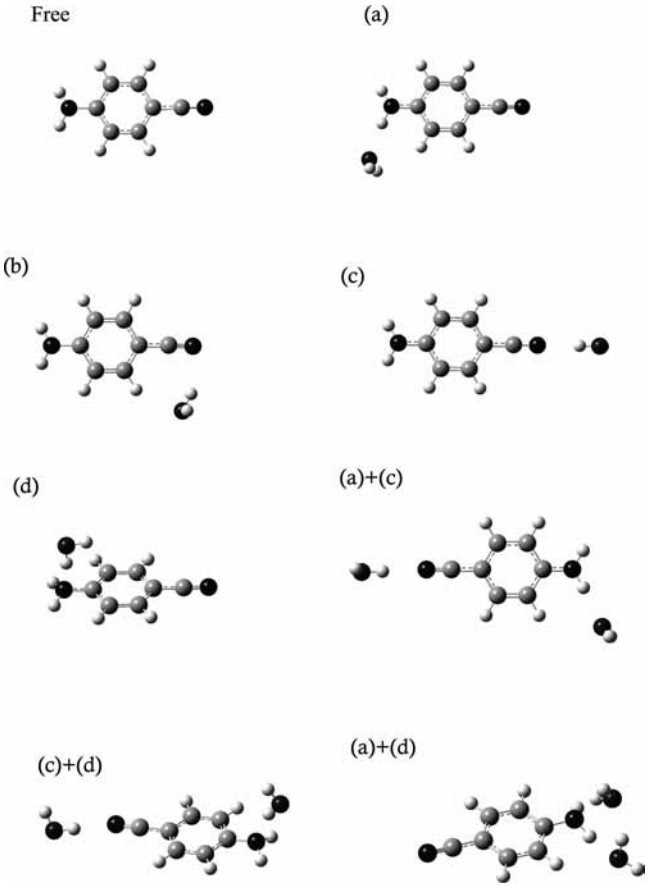

[a] (a) NH_2-donor conformer, (b) CN-side conformer, (c) CN-linear conformer, and (d) NH_2 acceptor conformer.

Quite similar water effects of (b)- and (c)-type clusters have also been reported on the jet-cooled clusters of BN and water.[30] Ishikawa et al. measured the vibrational frequency shift of the C≡N stretching mode of the BN cluster with several numbers of water molecules and found the low frequency shift for the 1:1 cluster and the high frequency shift for the 1:2 and 1:3 clusters. They performed ab initio calculations on the clusters and found frequency shifts of the C≡N frequency for the (b)- and (c)-type clusters similar to those of the present cases. They considered that the (b)-type cluster is most stable and that by adding the number of water molecules they form a ring structure to make the hydrogen bonding like a (c)-type cluster, which results in the high frequency shift. In this sense, it is an interesting issue how the frequency changes if one more water molecule is attached to the present cluster models. The selected configurations for the calculation of the C≡N frequency stretching mode are also shown in Scheme 2. As is seen from the result (Table 3), the calculated frequencies are almost the sum of the shift of each conformer up to two water molecules.

If the high frequency shift with decreasing temperature in water is due to the hydrogen bonding, the contribution of the clusters of (c) and (d) should increase relative to the cluster of (a). Because the stability of the cluster (b) is mainly attributed to the dipole−dipole interaction between water and ABN (antiparallel alignment of the dipole moment), we do not discuss this cluster further. To assess the change of the hydrogen bonding between water and ABN with changing the solvent density and temperature, we have performed MD simulations of ABN in water at different temperatures and densities (see section 2.3). Figure 11a−c shows the radial distribution functions (RDFs) $g(r)$ between water and ABN related to the hydrogen-bonding sites: (a) between H in $-NH_2$ of ABN and O in H_2O, (b) N in $-C\equiv N$ of ABN and H in H_2O, and (c) N in $-NH_2$ of ABN and H in H_2O, respectively. According to cluster model calculations, the type-(a) cluster is represented by Figure 11a, the type-(c) cluster by Figure 11b, and the type-(d) cluster by Figure 11c. In each case, the first peak of the RDF in the shortest distance corresponds to the hydrogen bonding between ABN and water. The hydrogen bonding in Figure 11c is the most sharply peaked among the three types.

We calculated the numbers of the hydrogen-bonded molecules by a numerical integration of the RDFs up to 2.4 Å. The results are shown in Table 5, and the relative change of the number of the hydrogen bonding to the value at 300 K is plotted against the solvent reduced density in Figure 12. The change seems to be monotonical, and no sharp difference is observed between the medium and the high density regions. We also calculated the relative change of the numbers of the hydrogen bonding to those in ambient condition by a different way using the following geometric definition of hydrogen bond:[52] (1) The distance between the oxygen atom of water and the donor sites of ABN is smaller than 3.6 Å. (2) The distance between the hydrogen atoms of water and the acceptor sites of ABN is smaller than 2.45 Å. (3) The angle between the hydrogen bond and OH bond of water or that of the hydrogen bond and NH bond of the amino group is smaller than 30°. The results from the above definitions are also shown by circles in Figure 12, and no significant differences from the estimation based on the RDFs are found, although the density dependence is somewhat larger in the geometrical definition, especially the hydrogen-bonding type (d).

A simple summation of these changes of the hydrogen bonding multiplied by the extent of the shift estimated by the DFT calculations reproduces the high frequency shift with

TABLE 4: Structural Information of ABN Obtained by the Geometry Optimization Using Cluster Model at the B3LYP/6-31+G(d,p) Level of the DFT Theory Using Gaussian 03[a]

structures	ΔE/kcal mol^{-1}	θ	L(C≡N)/Å	ν_{CN}/cm^{-1}	$\Delta\nu_{CN}$/cm^{-1}
(a)	–18.4470	15.73	1.1658	2318.05	–5.32
(b)	–15.3515	20.19	1.1662	2313.55	–9.82
(c)	–16.7220	18.76	1.1642	2330.24	+6.87
(d)	–10.7831	27.01	1.1647	2328.81	+5.44
(a) + (c)	–47.0154	12.38	1.1649	2324.27	+0.90
(a) + (d)	–36.5947	26.61	1.1650	2325.46	+2.19
(c) + (d)	–26.4759	26.41	1.1636	2335.98	+12.56

[a] ΔE, stabilization energy from the attachment of water molecules defined by $\Delta E = E$(cluster) $- E$(free ABN) $- E$(free water); θ, out-of-plane angle of the NH_2 group in deg; L(C≡N), C≡N bond length; ν_{CN}, calculated vibrational frequency of C≡N stretching mode; $\Delta\nu_{CN}$, frequency change of C≡N stretching mode from free ABN.

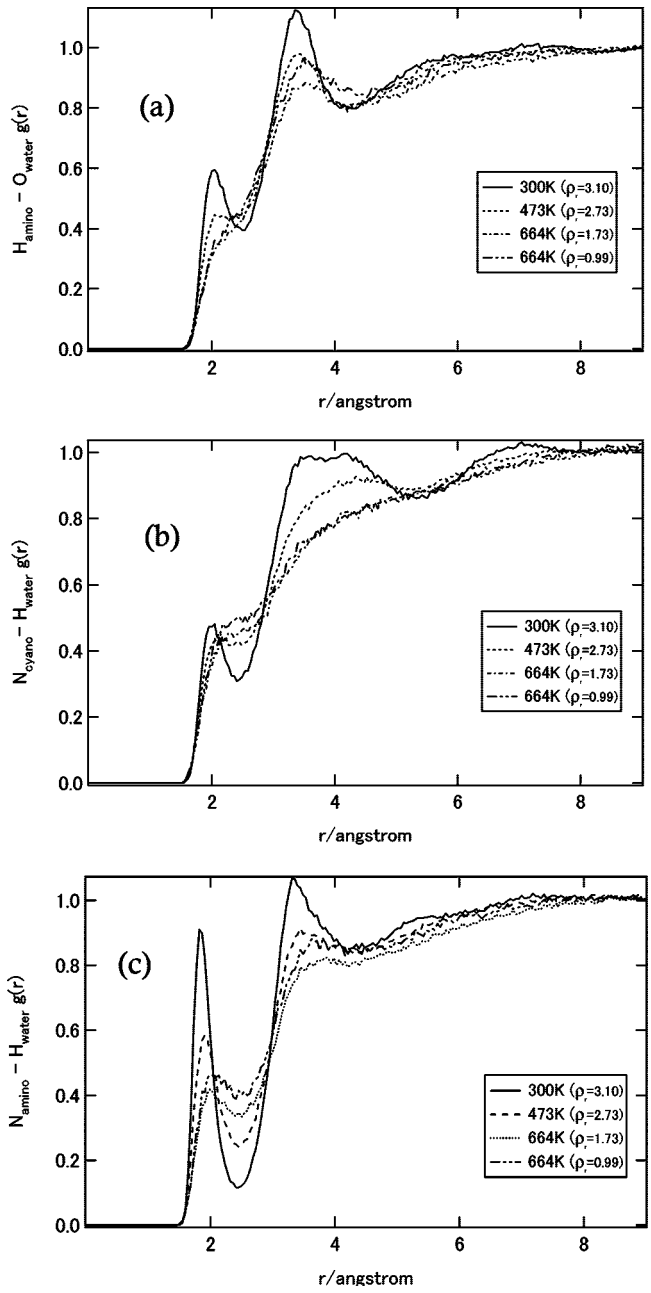

Figure 11. Radial distribution functions between (a) amino H of ABN and water O atoms, (b) cyano N of ABN and water H atoms, and (c) amino N of ABN and water H atoms, respectively.

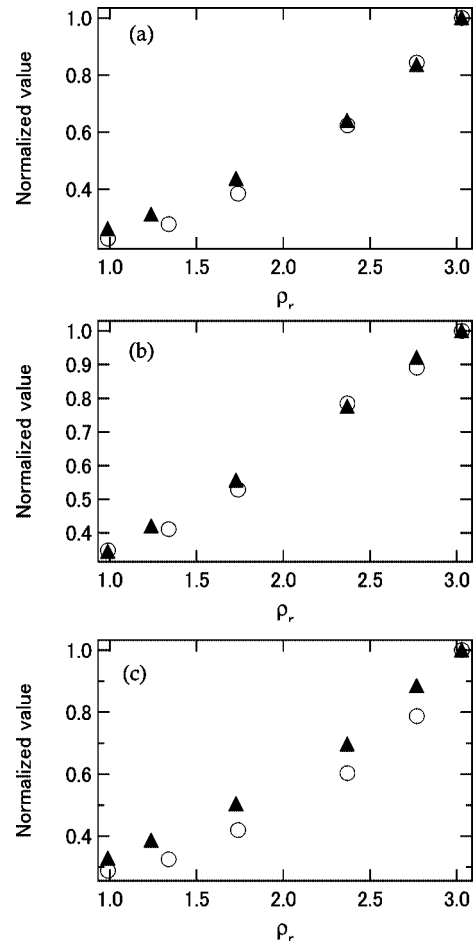

Figure 12. The changes of the number of hydrogen bonds from the ambient condition to the supercritical condition between (a) amino H of ABN and water O atoms, (b) cyano N of ABN and water H atoms, and (c) amino N of ABN and water H atoms: ▲, estimated from the integrations of first solvation shell (up to 2.4 Å); ○, estimated from the geometrical definition. See details in text.

TABLE 5: Coordination Numbers of Hydrogen Molecules Calculated from the Radial Distribution Functions[a]

ρ_r	T/K	$N_{NH2-H2O(a)}$	$N_{CN-H2O(c)}$	$N_{NH2-H2O(d)}$	$\Delta\nu_{calc}$/cm^{-1}
3.10	300	0.60	0.97	1.11	6.4
3.03	373	0.54	0.98	1.07	6.8
2.77	473	0.45	0.90	0.95	6.5
2.34	573	0.35	0.76	0.75	5.6
1.77	664	0.24	0.55	0.54	4.2
1.24	664	0.17	0.41	0.41	3.3
0.99	664	0.14	0.34	0.35	2.7

[a] ρ_r, T, reduced density and temperature set for MD simulation; $N_{NH2-H2O(a)}$, $N_{CN-H2O(c)}$, $N_{NH2-H2O(d)}$, coordination number of hydrogen bond obtained by integrating first peaks of radial distribution functions; $\Delta\nu_{calc}$, calculated vibrational frequency shift of C≡N stretching mode by using the results of DFT and MD simulation.

increasing solvent density (see Table 5). However, the dependence is somewhat smooth, and the model calculation cannot reproduce a large positive shift of the vibrational frequency specifically observed for water above $\rho_r \cong 2.8$. We consider that the present model is too simple to reproduce the experimental observations. For example, in our model MD calculation, we have not taken into account the electronic structure change by the solvent. Further, the frequency shift may not be proportional to those obtained by the cluster model if there are many solvent molecules around ABN. One plausible approach to this problem is application of the RISM-SCF method, in which the solvent molecules are treated explicitly.[53] By using the method, we are now trying to clarify the origin of the specific effect in water.

5. Conclusion

In this work, we have investigated the solvent effect on the C≡N stretching vibration of ABN in water, methanol, and cyclohexane by using Raman spectroscopy under the sub- and supercritical conditions, and acetonitrile under the subcritical conditions. The band peak position showed characteristic V-shape dependence on the density in all solvents that covered the supercritical region: that is, the peak frequency decreased with increasing density under the supercritical temperature, and

then around the medium density region of $\rho_r \approx 2$ the peak frequency increased with increasing density (or decreasing the temperature) along the isobar. The density dependence was most significant in water, especially near room temperature. The origin of the vibrational frequency shift was divided into four contributions: temperature ($\Delta\nu_T$), repulsive ($\Delta\nu_R$), attractive ($\Delta\nu_A$), and hydrogen-bonding effects ($\Delta\nu_{HB}$). The vibrational frequency shift in cyclohexane was well explained by the combination of $\Delta\nu_T + \Delta\nu_R + \Delta\nu_A$ using the hard-sphere theory for the repulsive effect and mean field approximation for the attractive effect. By subtracting $\Delta\nu_R$ and $\Delta\nu_T$ from the observed spectral shifts in water and methanol, $\Delta\nu_A + \Delta\nu_{HB}$ was extracted. The spectral shift from the low to the medium density region could be explained by the mean field attractive effect both in water and in methanol, which was supported by the linear correlation between the frequency shift and the CT absorption peak shift and by DFT calculations using PCM approach. To explain the high frequency shift observed in water above $\rho_r \cong 2.8$, however, we had to incorporate the effect of the hydrogen bonding. According to DFT calculations on the ABN cluster with water, the vibrational frequency shift was strongly dependent on the site of the hydrogen bonding. For the high frequency shift, a water molecule had to bind a specific site of a ABN molecule. We have also calculated the change of the hydrogen bonding between ABN and water using MD simulations based on the OPLA/AA potential model of ABN and SPC/E model water. Although the combinations of DFT calculations and MD simulations suggested the high frequency shift with increasing solvent density, the coincidence with the experimental observation was not satisfactory. More sophisticated treatment will be required to obtain a quantitative view on the effect of the hydrogen bonding such as the RISM-SCF method, and the work is now in progress.

Acknowledgment. This work was supported by Grants-in-Aid for Scientific Research from JSPS (No. 19350010).

Supporting Information Available: Relation between the Morse potential parameters and the harmonic and anharmonic frequencies calculated by VSCF. Table of the optimized vibrational frequencies in the fingerprint region of ABN−water clusters. Figures of the density dependence of Raman bandwidths of the C≡N stretching vibration, Raman spectra in the fingerprint region of ABN in water and methanol under sub- and supercritical regions, the density dependence of the vibrational frequencies of the ring stretching vibration, CH bending vibration, and phenyl−C≡N stretching vibration in water and methanol under sub- and supercritical regions, and the density dependence of the absorption bandwidth of ABN in water, methanol, cyclohexane, and acetonitrile under sub- and supercritical regions. This material is available free of charge via the Internet at http://pubs.acs.org.

References and Notes

(1) Weingärtner, H.; Franck, E. U. *Angew. Chem., Int. Ed.* **2005**, *44*, 2672.

(2) Bermejo, M. D.; Cocero, M. J. *AIChE J.* **2006**, *52*, 3933.

(3) Watanabe, M.; Sato, T.; Inomata, H.; Smith, R. L., Jr.; Arai, K.; Kruse, A.; Dinjus, E. *Chem. Rev.* **2004**, *104*, 5803.

(4) Genta, M.; Iwaya, T.; Sasaki, M.; Goto, M. *Waste Manage.* **2007**, *27*, 1167.

(5) Minami, E.; Saka, S. *J. Wood Sci.* **2003**, *49*, 73.

(6) (a) Yamaguchi, T.; Yoshida, K.; Yamamoto, N.; Hosokawa, S.; Inui, M.; Baron, A. Q. R.; Tsutsui, S. *J. Phys. Chem. Solids* **2005**, *66*, 2246. (b) Yamaguchi, T.; Benmore, C. J.; Soper, A. K. *J. Chem. Phys.* **2000**, *112*, 8976.

(7) (a) Matubayasi, N.; Wakai, C.; Nakahara, M. *J. Chem. Phys.* **1997**, *107*, 9133; **1999**, *110*, 8000. (b) Matubayasi, N.; Nakao, N.; Nakahara, M. *J. Chem. Phys.* **2001**, *114*, 4107.

(8) (a) Hoffmann, M. M.; Conradi, M. S. *J. Am. Chem. Soc.* **1997**, *119*, 3811. (b) Hoffmann, M. M.; Conradi, M. S. *J. Phys. Chem. B* **1998**, *102*, 263.

(9) (a) Tassaing, T.; Danten, Y.; Besnard, M. *J. Mol. Liq.* **2002**, *101*, 149. (b) Lalanne, P.; Andanson, J. M.; Soetens, J. C.; Tassaing, T.; Danten, Y.; Besnard, M. *J. Phys. Chem. A* **2004**, *108*, 3902.

(10) Ikushima, Y.; Hatakeda, K.; Saito, N.; Arai, K. *J. Chem. Phys.* **1998**, *108*, 5855.

(11) (a) Asahi, N.; Nakahara, M. *Chem. Phys. Lett.* **1998**, *290*, 63. (b) Asahi, N.; Nakahara, M. *J. Chem. Phys.* **1998**, *109*, 1319.

(12) (a) Bennett, G. E.; Johnston, K. P. *J. Phys. Chem.* **1994**, *98*, 441. (b) Niemeyer, E. D.; Dunbar, R. A.; Bright, F. V. *Appl. Chem.* **1997**, *51*, 1547. (c) Minami, K.; Mizuta, M.; Suzuki, M.; Aizawa, T.; Arai, K. *Phys. Chem. Chem. Phys.* **2006**, *8*, 2257. (d) Kometani, N.; Takemiya, K.; Yonezawa, Y.; Amita, F.; Kajimoto, O. *Chem. Phys. Lett.* **2004**, *394*, 85. (e) Osada, M.; Toyoshima, K.; Mizutani, T.; Minami, K.; Watanabe, M.; Adschiri, T.; Arai, K. *J. Chem. Phys.* **2003**, *118*, 4573. (f) Mikami, K.; Ohashi, T.; Suzuki, M.; Aizawa, T.; Adshjiri, T.; Arai, T. *Anal. Sci.* **2006**, *22*, 1417.

(13) Lu, J.; Boughner, E. C.; Liotta, C. L.; Eckert, C. A. *Fluid Phase Equilib.* **2002**, *198*, 37.

(14) Aizawa, T.; Kanakubo, M.; Hiejima, Y.; Ikushima, Y.; Smith, R. L., Jr. *J. Phys. Chem. A* **2005**, *109*, 7353.

(15) Xiang, T.; Johnston, K. P. *J. Phys. Chem.* **1994**, *98*, 7915.

(16) Blugarevich, D. S.; Sako, T.; Sugeta, T.; Ohtake, K.; Takebayashi, Y.; Kamizawa, C. *J. Chem. Phys.* **1999**, *111*, 4239.

(17) Oka, H.; Kajimoto, O. *Phys. Chem. Chem. Phys.* **2003**, *5*, 2535.

(18) (a) Fujisawa, T.; Terazima, M.; Kimura, Y.; Maroncelli, M. *Chem. Phys. Lett.* **2006**, *430*, 303. (b) Fujisawa, T.; Terazima, M.; Kimura, Y. *J. Phys. Chem. A* **2008**, *112*, 5515.

(19) (a) Gibson, E. M.; Jones, A. C.; Taylor, A. G.; Bouwman, W. G.; Phillips, D.; Sandell, J. *J. Phys. Chem.* **1988**, *92*, 528. (b) Yu, H.; Joslin, E.; Crystall, B.; Smith, T.; Sinclair, W.; Phillips, D. *J. Phys. Chem.* **1993**, *97*, 8146.

(20) (a) Alejandro, E.; Fernández, J. A.; Fernando, C. *Chem. Phys. Lett.* **2002**, *353*, 195. (b) Alejandro, E.; Landajo, C.; Longarte, A.; Fernández, J. A.; Fernando, C. *J. Chem. Phys.* **2003**, *119*, 9513.

(21) Gibson, E. M.; Jones, A. C.; Phillips, D. *Chem. Phys. Lett.* **1988**, *146*, 270.

(22) (a) Sakota, K.; Yamamoto, N.; Ohashi, K.; Sekiya, H.; Saeki, M.; Ishiuchi, S.; Sakai, M.; Fujii, M. *Chem. Phys. Lett.* **2001**, *341*, 70. (b) Sakota, K.; Yamamoto, N.; Ohashi, K.; Saeki, M.; Ishiuchi, S.; Sakai, M.; Fujii, M.; Sekiya, H. *Chem. Phys.* **2002**, *281*, 209. (c) Sakota, K.; Yamamoto, N.; Ohashi, K.; Saeki, M.; Ishiuchi, S.; Sakai, M.; Fujii, M.; Sekiya, H. *Phys. Chem. Chem. Phys.* **2003**, *5*, 1775.

(23) (a) Lommatzsch, U.; Brutschy, B. *Chem. Phys.* **1998**, *234*, 35. (b) Krau*β*, O.; Lommatzsch, U.; Lahmann, C.; Brutschy, B.; Retting, W.; Herbich, J. *Phys. Chem. Chem. Phys.* **2001**, *3*, 74.

(24) (a) Jiang, S.; Levy, D. H. *J. Phys. Chem. A* **2002**, *106*, 8590. (b) Jiang, S.; Levy, D. H. *J. Phys. Chem. A* **2003**, *107*, 6785.

(25) Khakk, O. S.; Meeks, J. L.; McGlynn, S. P. *Chem. Phys. Lett.* **1976**, *39*, 457.

(26) Rettig, W.; Wermuth, G.; Lippert, E. *Ber. Bunsen-Ges. Phys. Chem.* **1979**, *83*, 692.

(27) Leinhos, U.; Kühnle, W.; Zachariasse, K. A. *J. Phys. Chem.* **1991**, *95*, 2013.

(28) Kawski, A.; Kukliński, B.; Bojarski, P. *Chem. Phys. Lett.* **2006**, *425*, 257.

(29) Dahl, K.; Biswas, R.; Ito, N.; Marocncelli, M. *J. Phys. Chem. B* **2005**, *109*, 1563.

(30) Ishikawa, S.; Ebata, T.; Mikami, N. *J. Chem. Phys.* **1999**, *110*, 9504.

(31) Eaton, G.; Pena-Nu, S. A.; Symons, R. C. M. *J. Chem. Soc., Faraday Trans.* **1988**, *84*, 2181.

(32) Ben-Amotz, D.; Lee, M. R.; Cho, S. Y.; List, D. J. *J. Chem. Phys.* **1992**, *96*, 8781.

(33) Reimers, R. J.; Hall, E. L. *J. Am. Chem. Soc.* **1999**, *121*, 3730.

(34) Akimoto, S.; Kajimoto, O. *Chem. Phys. Lett.* **1993**, *209*, 263.

(35) (a) Fujisawa, T.; Maru, E.; Amita, F.; Harada, M.; Uruga, T.; Kimura, Y. *Water, Steam, and Aqueous Solutions for Electric Power*; Proceedings of the 14th International Conference on the Properties of Water and Steam, Kyoto, 2004; p 445. (b) Kimura, Y.; Amita, F.; Fujisawa, T. *Rev. High Pressure Sci. Technol.* **2006**, *16*, 87.

(36) (a) de Reuck, K. M.; Craven, R. J. B. *Methanol/International Thermodynamic Tables of the Fluid State-12, IUPAC*; Blackwell Scientific Pub.: Oxford, 1993. (b) Marshall, W. L.; Franck, E. U. *J. Phys. Chem. Ref. Data* **1981**, *10*, 295. (c) Penoncello, S. G.; Jacobsen, R. T.; Goodwin, A. R. H. *Int. J. Thermophys.* **1995**, *16*, 519. (d) Francesconi, A. Z.; Franck, E. U.; Lentz, H. *Ber. Phys. Chem.* **1975**, *10*, 897.

(37) Frisch, M. J.; Trucks, G. W.; Schlegel, H. B.; Scuseria, G. E.; Robb, M. A.; Cheeseman, J. R.; Montgomery, J. A., Jr.; Vreven, T.;

Kudin, K. N.; Burant, J. C.; Millam, J. M.; Iyengar, S. S.; Tomasi, J.; Barone, V.; Mennucci, B.; Cossi, M.; Scalmani, G.; Rega, N.; Petersson, G. A.; Nakatsuji, H.; Hada, M.; Ehara, M.; Toyota, K.; Fukuda, R.; Hasegawa, J.; Ishida, M.; Nakajima, T.; Honda, Y.; Kitao, O.; Nakai, H.; Klene, M.; Li, X.; Knox, J. E.; Hratchian, H. P.; Cross, J. B.; Bakken, V.; Adamo, C.; Jaramillo, J.; Gomperts, R.; Stratmann, R. E.; Yazyev, O.; Austin, A. J.; Cammi, R; Pomelli, C.; Ochterski, J. W.; Ayala, P. Y.; Morokuma, K.; Voth, G. A.; Salvador, P.; Dannenberg, J. J.; Zakrzewski, V. G.; Dapprich, S.; Daniels, A. D.; Strain, M. C.; Farkas, O.; Malick, D. K.; Rabuck, A. D.; Raghavachari, K.; Foresman, J. B.; Ortiz, J. V.; Cui, Q.; Baboul, A. G.; Clifford, S.; Cioslowski, J.; Stefanov, B. B.; Liu, G.; Liashenko, A.; Piskorz, P.; Komaromi, I.; Martin, R. L.; Fox, D. J.; Keith, T.; Al-Laham, M. A.; Peng, C. Y.; Nanayakkara, A.; Challacombe, M.; Gill, P. M. W.; Johnson, B.; Chen, W.; Wong, M. W.; Gonzalez, C.; Pople, J. A. *Gaussian 03*; Gaussian, Inc.: Wallingford, CT, 2004.

(38) Tomasi, J.; Persico, M. *Chem. Rev.* **1994**, *94*, 2027.

(39) A sphere was also placed on the hydrogen atom of the NH_2 group in the PCM calculation.

(40) (a) Schmidt, M. W.; Bladridge, K. K.; Boatz, J. A.; Elbert, S. T.; Gordon, M. S.; Jensen, J. H.; Koseki, S.; Matsunaga, N.; Nguyen, K. A.; Su, S.; Windus, T. L.; Dupuis, M.; Montgomery, J. A. *J. Comput. Chem.* **1993**, *14*, 1347. (b) Gordon, M. S.; Schmidt, M. W. In *Theory and Applications of Computational Chemistry: the first forty years*; Dykstra, C. E., Frenking, G., Kim, K. S., Scuseria, G. E., Eds.; Elsevier: Amsterdam, 2005; p 1167.

(41) Plimpton, S. J. *J. Comput. Phys.* **1995**, *117*, 1. (http://lammps.sandia.gov).

(42) Berendsen, H. J. C.; Gregera, J. R.; Straatsma, T. P. *J. Phys. Chem.* **1987**, *91*, 6269.

(43) (a) Rizzo, R. C.; Jorgensen, W. L. *J. Am. Chem. Soc.* **1999**, *121*, 4827. (b) Price, M. L. P.; Ostrovsky, D.; Jorgensen, W. L. *J. Comput. Chem.* **2001**, *22*, 1340.

(44) Fini, G.; Mirone, P. *Spectrochim. Acta* **1976**, *32A*, 439.

(45) Inaba, R.; Okamoto, H.; Yoshihara, K.; Tasumi, M. *Chem. Phys. Lett.* **1991**, *185*, 56.

(46) Fawcett, W. R.; Liu, G.; Kessler, T. E. *J. Phys. Chem.* **1993**, *97*, 9293.

(47) Tucker, S. C. *Chem. Rev.* **1999**, *99*, 391.

(48) Kimura, Y.; Hirota, N. *J. Chem. Phys.* **1999**, *111*, 5474.

(49) In the original papers, the effect of the centrifugal distortion has been included. The effect was estimated to be small (ca. 0.5 cm^{-1}) and independent of the solvent. Therefore, we neglected the term here.

(50) See, for example: Reichardt, C. *Solvents and Solvents Effects in Organic Chemistry*; VCH: Weinheim, 1988.

(51) Ben-Amotz, D.; Herschbach, D. R. *J. Phys. Chem.* **1990**, *94*, 1038.

(52) Marti, J.; Padro, A. J.; Guardia, E. *J. Chem. Phys.* **1996**, *105*, 639.

(53) (a) Sato, H.; Hirata, F.; Kato, S. *J. Chem. Phys.* **1996**, *105*, 1546. (b) Sato, H. In *Molecular Theory of Solvation*; Hirata, F., Ed.; Kluwer Academic Publishers: Dordrecht, Hardbound, 2003; Chapter 2. (c) Yokogawa, D.; Sato, H.; Sakaki, S. *J. Chem. Phys.* **2007**, *126*, 244504. (d) Sato, H. In *Continuum Solvation Models in Chemical Physics: From Theory to Applications*; Mennucci, B., Cammi, R., Eds.; John Wiley & Sons Inc.: New York, 2008.

JP8111606